ISSN 0015-4628, Fluid Dynamics, 2013, Vol. 48, No. 6, pp. 827–836. © Pleiades Publishing, Ltd., 2013.
Original Russian Text © O.A. Druzhinin, Yu.I. Troitskaya, 2013, published in Izvestiya Rossiiskoi Akademii Nauk, Mekhanika Zhidkosti i Gaza, 2013, Vol. 48, No. 6, pp. 135–146.

Internal Wave Radiation by a Turbulent Fountain in a Stratified Fluid

O. A. Druzhinin and Yu. I. Troitskaya

Received October 26, 2012

Abstract—Large eddy simulation is applied to model a fountain in a density-stratified fluid. The fountain is formed, as a vertical turbulent jet penetrates through a pycnocline. The jet flow is initiated by the formulation of a boundary condition in the form of an upward neutral-buoyancy fluid flow with the Gaussian axisymmetric mean-velocity profile and a given fluctuation level. It is shown that at a Froude number Fr higher than a certain critical value the fountain executes self-oscillations accompanied by internal wave generation within the pycnocline. The predominant self-oscillation mode is axisymmetric, when the fountain top periodically breaks down generating internal wave packets traveling toward the periphery of the computation domain. The characteristic frequency of the internal waves coincides with that of the fountain top oscillations and monotonically decreases with increase in Fr. The Fr-dependence of the fountain top oscillation amplitude obtained in the numerical solution is in good agreement with the predictions of the theoretical Landau model for the instability mode in the soft self-excitation regime.

Keywords: stratification, submerged buoyant jet, pycnocline, turbulence, self-oscillations, internal waves.

DOI: 10.1134/S0015462813060136

A heavy-fluid jet having an initial upward-directed momentum and propagating in a lighter fluid is called a fountain. The jet is decelerated under the action of the buoyancy force (gravity) and reaches a maximum height (turn point), whereupon the fluid flows downward from the turn point, thus forming a counter stream, and spreads radially on its buoyancy level. The fountain dynamics attracts an interest thanks to many applications in hydrodynamics and geophysics [1].

A flow similar with a fountain can be formed in a fluid with a nearly two-layer stratification, when the light fluid is introduced in the lower fluid layer at a certain distance from the density jump (pycnocline). In this case, even in the absence of an initial momentum, the fluid accelerates under the action of the buoyance force and acquires a positive vertical momentum. In the case of a turbulent fountain, the entrainment of the surrounding fluid leads to a situation, when the floating-up fluid approaching the pycnocline has a density similar in value with that of the fluid in the lower layer. Thus, a fluid jet of neutral buoyancy (with respect to the lower-layer fluid) with a nonzero vertical momentum is formed. If its velocity is fairly high, then the heavy fluid jet penetrates in the region above the pycnocline, thus forming a fountain. Such fountains can arise, for example, when waste water jets float up in the ocean near underwater collectors in the presence of a seasonal pycnocline [2–4].

Another important example of these fountains is furnished by jets consisting of gas bubbles which emanate from fractures at the ocean bottom. A similar phenomenon might also be expected in the proximity of underwater sources of fresh water.

The fountain dynamics were studied both in physical laboratory experiments and in numerical simulations [5–7]. The results of these studies have shown that the jet dynamics are determined by the Froude Fr and Reynolds Re numbers based on the axial velocity and jet diameter, the buoyancy jump, and the kinematic viscosity of the fluid. At low Fr and Re the fountain represents a steady flow which loses stability with increase in these parameters. Depending on Fr and Re, different unstable modes of fountain oscillations can be self-excited.

The fountain oscillations are capable of radiating internal waves if the oscillation frequency is lower than the buoyancy frequency. In turn, the manifestation of these internal waves on the water surface might be expected, which makes possible the distant diagnostics of underwater buoyant jets. The experimental indications of the possibility of surface manifestation of the internal waves excited by underwater collectors of waste water are presented in [3]. The internal waves generated by the interaction between a buoyant jet and a pycnocline were detected in the laboratory experiment [8], in which the condition of the scale modeling with respect to the Froude number was fulfilled for a typical coastal disposal system. The results obtained show that internal waves can be generated in the pycnocline under the action of buoyant jets. The results of laboratory experiments and a theoretical analysis [9] have shown that a buoyant jet interacting with a pycnocline executes quasiperiodic oscillations in the vertical plane which effectively generate internal waves. It was established that the internal wave source is the axisymmetric global mode of the jet oscillations. We note that an analogous situation can arise in the case of submerged fountain outflow onto the free surface. For example, the laboratory experiments [10, 11] showed that surface waves can be generated by a plane submerged fountain.

Direct numerical simulation of a fountain formed in the case of laminar, heavy-fluid jet penetration through a pycnocline showed that at the Froude number higher than a certain critical value the flow becomes unstable and the fountain executes self-oscillations accompanied by internal wave generation in the pycnocline [12]. In the frequency spectrum of the internal waves the main peak coincides with the fountain top oscillation frequency which monotonically diminishes with increase in Fr. The Fr-dependence of the fountain top oscillation amplitude obtained in the numerical simulation is in good agreement with the predictions of the theoretical model of the competition between interacting modes in the soft self-excitation regime.

It should be noted that in the above-listed studies the Reynolds number considered was relatively low ($\mathrm{Re} < 10^4$ in the laboratory experiments and $\mathrm{Re} < 10^3$ in the numerical experiments). However, in practice (for example, in geophysical applications) the Reynolds number is usually fairly high ($\mathrm{Re} > 10^5$) and the flows are turbulent.

The purpose of this study is to numerically model the dynamics of a fountain generated when a vertical turbulent jet penetrates through a pycnocline at Reynolds numbers similar in value to the actual ($\mathrm{Re} \sim 10^5$) using large eddy simulation.

1. BASIC EQUATIONS AND DESCRIPTION OF THE NUMERICAL METHOD

We will consider a fluid with stable density stratification, with a density jump (pycnocline) located on a certain horizon $Z = Z_0$. The density profile is given in the form:

$$R_0(Z) = \rho_0\left(1 + 0.5\frac{\Delta\rho}{\rho_0}\left[1 - \tanh\frac{2(Z - Z_0)}{D_0}\right]\right).$$

A jet with the mean density profile

$$u(x, y, t) = U_0 \exp\left(-4(x^2 + y^2)\right) \tag{1.1}$$

flows vertically upward through the lower boundary $Z = 0$.

Under the action of buoyancy forces the jet is decelerated in the vicinity of the pycnocline, curves it, and penetrates into the upper layer of the lighter fluid at a certain finite height (up to the turn point). Then, similarly to the flow in a conventional fountain, the fluid in the jet flows downward from the turn point, thus forming a counter stream, and then spreads radially in a plane on the neutral buoyancy horizon.

The dimensionless variables are determined as follows:

$$(x,\ y,\ z) = \frac{(X,\ Y,\ Z)}{D_0}, \qquad U_i = \frac{u_i}{U_0}, \qquad \rho = \frac{R\ -\ R_0(z)}{\Delta\rho},$$

where u_i are the components of the velocity vector ($i = x,\ y,\ z$) and R is the fluid density.

The fluid dynamics equations were integrated using large eddy simulation. In this method the instantaneous velocity and density fields are represented as the sums of large-scale (or filtered) fields and subgrid fluctuations. The fluctuation effect on the large-scale field dynamics (that is, the Reynolds stresses) is taken into account using different closure hypotheses (see [13] for an overview of the LES methods).

For the large-scale fields the LES-filtered Navier–Stokes equations in the Boussinesq approximation and the fluid incompressibility condition in the dimensionless variables take the form:

$$\frac{\partial U_i}{\partial t}\ +\ U_j\frac{\partial U_i}{\partial x_j} = -\frac{\partial P}{\partial x_i}\ +\ \frac{1}{\mathrm{Re}}\frac{\partial^2 U_i}{\partial x_j^2}\ -\ \frac{\partial \tau_{ij}}{\partial x_j}\ -\ \frac{\delta_{ij}}{\mathrm{Fr}^2}\rho, \tag{1.2}$$

$$\frac{\partial U_j}{\partial x_j} = 0,$$

where δ_{ij} is the Kronecker symbol. The equation for the fluid density field can be written in the form:

$$\frac{\partial \rho}{\partial t}\ +\ U_j\frac{\partial \rho}{\partial x_j}\ +\ U_z\frac{d\rho_{\mathrm{ref}}}{dz} = \frac{1}{\mathrm{Re}\,\mathrm{Pr}}\frac{\partial^2 \rho}{\partial x_j^2}\ -\ \frac{\partial \tau_{\rho j}}{\partial x_j}, \tag{1.3}$$

where the fluxes (Reynolds stresses) τ_{ij} and $\tau_{\rho j}$ are modeled using the closure procedure discussed below. In Eq. (1.3) the original profile of the dimensionless density is as follows:

$$\rho_{\mathrm{ref}}(z) = 1\ +\ 0.5\big[1\ -\ \tanh 2(z\ -\ z_0)\big], \tag{1.4}$$

where $z_0 = Z_0/D_0$ is the pycnocline horizon. In Eq. (1.3) the variation in $\rho_{\mathrm{ref}}(z)$ due to molecular diffusion is neglected. In Eq. (1.2) the Reynolds (Re) and Froude (Fr) numbers are determined as follows:

$$\mathrm{Re} = \frac{U_0 D_0}{\nu}, \qquad \mathrm{Fr} = \frac{U_0}{N_0 D_0}, \tag{1.5}$$

$$N_0 = \left(-\frac{g}{\rho_0}\frac{dR_0}{dZ}\right)^{1/2} = \left(\frac{g}{\rho_0}\frac{\Delta\rho}{D_0}\right)^{1/2},$$

where ν is the kinematic viscosity of the fluid and N_0 is the dimensional buoyancy frequency at the center of the pycnocline. From Eqs. (1.2)–(1.4) it follows that at the center of the pycnocline the dimensionless buoyancy frequency $N_m = 1/\mathrm{Fr}$.

In this study we use the LES closure model based on the equation for the kinetic energy of the subgrid turbulence, $k = 1/2\tau_{ij}$ [14, 15]. The equation for k is written in the form:

$$\frac{\partial k}{\partial t}\ +\ U_j\frac{\partial k}{\partial x_j} = \frac{\partial}{\partial x_i}\left(\nu_i\frac{\partial k}{\partial x_j}\right)\ +\ \nu_t\left(\frac{\partial U_i}{\partial x_j}\ +\ \frac{\partial U_j}{\partial x_i}\right)\frac{\partial U_i}{\partial x_j}\ -\ c_1\frac{k^{3/2}}{l}\ +\ \frac{\nu_t}{\mathrm{Fr}^2}\left(\frac{d\rho_{\mathrm{ref}}}{dz}\ +\ \frac{\partial \rho}{\partial z}\right), \tag{1.6}$$

where turbulent viscosity is specified in the form:

$$\nu_t = c_2 l k^{1/2}. \tag{1.7}$$

In Eq. (1.7) $c_1 = 0.1$ and $c_2 = 0.93$ are constant coefficients, while the scale length l is taken to be equal to the spatial step of the grid. The fluxes τ_{ij} and $\tau_{j\rho}$ are expressed in the form:

$$\tau_{ij}\ -\ \frac{1}{3}\tau_{kk} = -\nu_t\left(\frac{\partial U_i}{\partial x_j}\ +\ \frac{\partial U_j}{\partial x_i}\right), \tag{1.8}$$

$$\tau_{\rho j} = -\frac{\nu_t}{\mathrm{Pr}_t}\frac{\partial \rho}{\partial x_j}. \tag{1.9}$$

In this study Pr and Pr_t are taken to be equal to unity.

Equations (1.2), (1.3), and (1.6) are solved in a rectangular domain with the following dimensions: $-30 \le x \le 30$, $-30 \le y \le 30$, and $0 \le z \le 30$. On the lateral vertical boundaries of the computation domain $x = \pm 30$ in the (y, z) plane and on the upper horizontal boundary $z = 30$ in the (x, y) plane the von Neumann conditions (zero displacement) are imposed for all the variables. On the lower boundary $z = 0$ in the (x, y) plane the condition for the velocity corresponds to the upward directed jet with neutral buoyancy (relative to the surrounding fluid) with the Gaussian profile (1.1), on which the fluctuations of the form

$$U_i^b(x, y, t) = \exp(-4(x^2 + y^2))(\delta_{iz} + U_{fi}(x, y, t)) \tag{1.10}$$

are superimposed.

The fluctuation field U_{fi} is represented in the form of the sum of independent Fourier harmonics with random phases and a homogeneous broad spatial-temporal spectrum and an amplitude of 30% of the mean axial velocity. The fluctuation amplitude is taken to be fairly large in order to accelerate in a maximum degree jet flow transition to the developed turbulence regime. This is due to the limited dimensions of the computation domain in the vertical direction. The von Neumann boundary condition is preassigned for the density. The jet Reynolds number is taken to be 8×10^4 and at a distance of about ten original diameters from the lower boundary the jet flow becomes turbulent. The value z_0 in Eq. (1.4) determining the pycnocline horizon is taken to be fairly large (15 in the dimensionless length units), such that the effect of the transitional processes connected with the attainment of turbulent flow in the jet produced by the boundary condition (1.10) can be neglected.

Equations (1.2), (1.3), and (1.6) are discretized using a second-order finite-difference method on a uniform staggered grid consisting of $400 \times 400 \times 200$ gridpoints in the x, y, and z coordinates, respectively. The integration is performed using the Adams–Bashforth second-order method [12] with the time step $\Delta t = 0.015$. The splitting method [16] is used and the Poisson equation for the pressure is solved using the cosine transformation in the x and y coordinates (fast Fourier transformation) and the Gauss method in the z coordinate.

As can be seen from the numerical results presented below, the fountain generates internal waves propagating in the pycnocline toward the computation domain boundaries (vertical planes (y, z) at $x = \pm 30$ and (x, z) at $y = \pm 30$). To avoid the internal wave reflection from the vertical boundaries the terms $[-F(x, y)U_z]$ and $[-F(x, y)\rho]$ are added to the right sides of Eqs. (1.2) and (1.3), where the function $F(x, y) = 1$ in a narrow layer (one dimensionless length unit in thickness) near the vertical boundaries and vanishes in the rest of the computation domain. Thus, the internal wave decay on the boundaries is achieved and the reflected wave effect can be neglected [17].

2. RESULTS OF THE NUMERICAL MODELING

Numerical simulation was carried out for the Froude number values in the jet entry section ($z = 0$) on the range $0 < \mathrm{Fr}(0) < 20$ and at $\mathrm{Re} = 8 \times 10^4$ at the same boundary conditions discussed above. At the initial moment of time the velocity and density fields $U(x, y, z)$ and $\rho(x, y, z)$ were taken to be zero. Then the boundary condition for the velocity (1.10) was "turned on" adiabatically (in proportion to the factor $1 - \exp(-t)$, where t is time). After transitional processes have been terminated, the statistically steady distribution of the velocity and density fields was attained to the moment $t \approx 800$. Starting from this moment the time-average fields and r.m.s. fluctuations were calculated and the data for calculating the temporal spectra of the fluctuations were stored. The calculations were made on the time interval $800 < t < 1800$ including not less than 5 or 6 periods of the internal waves generated within the pycnocline.

At fairly small z ($z < z_0$) the stratification effect is slight and the jet propagates in an almost density-homogeneous fluid. Since the Reynolds number is fairly high ($\mathrm{Re} = 8 \times 10^4$), under the action of the initial fluctuations the jet becomes turbulent fairly rapidly (at a distance of a few diameters in z). In Fig. 1a we have plotted the profiles of the mean velocity $\langle U_z(x, 0, z)\rangle$ obtained in the numerical simulation for different

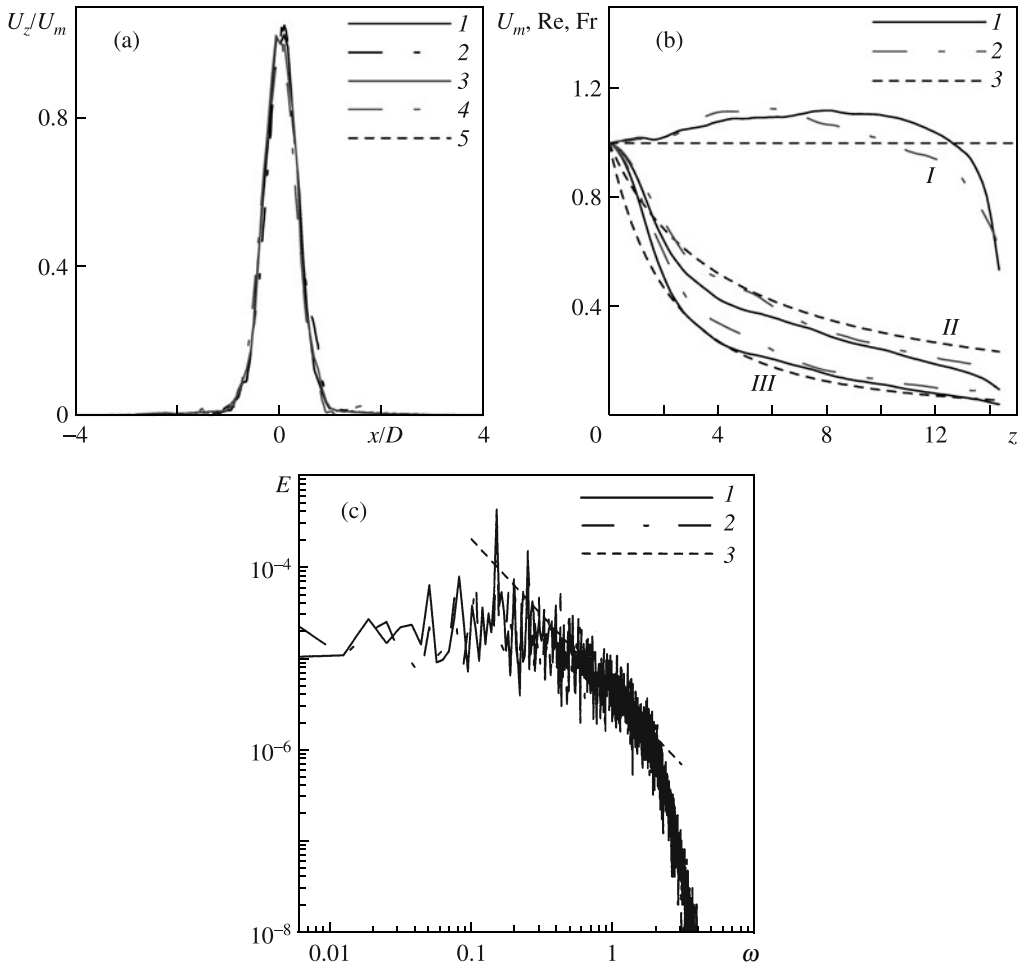

Fig. 1. Profiles of the mean vertical velocity component $\langle U_z(x,\ 0)\rangle$ for Fr(0) = 5 and 15 at different z (a), z-dependences of the mean axial velocity (*I*) and the Reynolds (*II*) and Froude (*III*) numbers (b), and frequency spectrum of the velocity fluctuations (c) for different Fr: (a) (*1*) $z = 3$, Fr(0) = 5; (*2*) $z = 12$, Fr(0) = 5; (*3*) $z = 3$, Fr(0) = 15; (*4*) $z = 12$, Fr(0) = 15; and (*5*) (2.2); (b) (*1*) Fr(0) = 3; (*2*) Fr(0) = 15; and (*3*) (2.3); and (c) (*1*) Fr(0) = 15 and (*3*) $\omega^{-5/3}$.

Froude numbers and normalized by the axial velocity $\langle U_z(0,\ 0,\ z)\rangle$ and the jet diameter, which at different distances in z is calculated as follows:

$$D(z) = \frac{2}{\sqrt{\pi}}\,\frac{1}{\langle U_z(0,\ 0,\ z)\rangle}\int\limits_{L_x}^{L_x}\langle U_z(x,\ 0,\ z)\rangle\,dx. \tag{2.1}$$

The velocity profiles are well described by the self-similar solution [17]

$$\langle U_z(x,\ y,\ z)\rangle = U_m(z)\exp\left(-4\frac{x^2 + y^2}{D^2(z)}\right), \tag{2.2}$$

where $U_m(z) = \langle U_z(0,\ 0,\ z)\rangle$. The dependences of the axial velocity and Re and Fr on z normalized by their corresponding initial values at $z = 0$ are presented in Fig. 1b. In a region fairly far from the pycnocline ($z < 12$) these dependences are well described by the expressions

$$U_m(z) = \frac{U(0)D(0)}{0.23z + 1}, \qquad \mathrm{Re}(z) = \mathrm{Re}(0), \qquad \mathrm{Fr}(z) = \frac{\mathrm{Fr}(0)}{(0.23z + 1)^2}, \tag{2.3}$$

which follow from the conservation law for the momentum flux of a turbulent let with the expansion coefficient 0.23. This coefficient is similar in value to the conventional value 0.22 for the axisymmetric turbulent submerged jet [18].

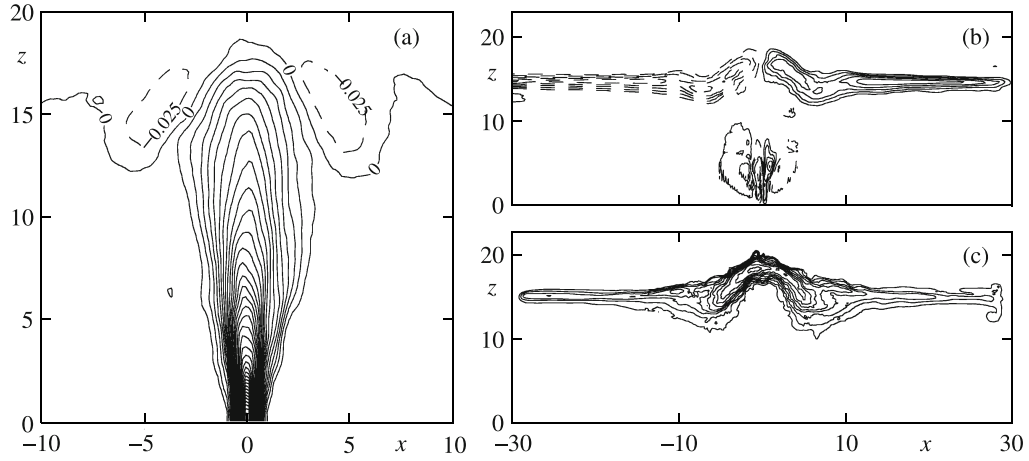

Fig. 2. Distributions of the mean vertical $\langle U_z \rangle$ (a) and horizontal $\langle U_x \rangle$ (b) velocity components and r.m.s. density fluctuations ρ' (c) in the central $(x,\ z)$ plane for $\mathrm{Fr}(0) = 15$; the isoline increments are 0.025, 0.01, and 0.04 for (a–c).

In Fig. 1c the frequency spectrum of the jet velocity fluctuations $E(\omega)$ is presented; it was obtained in the numerical simulation with $\mathrm{Fr}(0) = 15$. The spectrum was calculated and averaged from five time realizations at five points with the coordinates $(x = 0,\ y = 0,\ z = 12)$, $(x = 0,\ y = \pm 0.45,\ z = 12)$, and $(x = \pm 0.45,\ y = 0,\ z = 12)$. Clearly that the spectrum is well described by the Kolmogorov asymptotics $\omega^{-5/3}$, characteristic of the developed turbulence, on the frequency range $0.2 < \omega < 2$. The calculations for different Froude numbers show that the spectra are almost independent of Fr.

The results presented in Fig. 1b, together with asymptotics (2.3), show that Fr rapidly diminishes with increase in z. Thus, as the pycnocline is approached, the local value $\mathrm{Fr}(z)$ is considerably smaller than the initial value $\mathrm{Fr}(0)$. For this reason, it was the value $\mathrm{Fr} = \mathrm{Fr}(12)$ that was taken as the near-pycnocline jet flow characteristic directly determining the fountain properties. It should also be noted that the self- similar solution (2.2), (2.3) performs well in the region fairly far from the pycnocline, at $z < 12$. At $\mathrm{Fr}(0) > 15$ the fountain oscillation amplitude is fairly high (of the order of unity) and the fountain dynamics change the jet properties near the pycnocline. Because of this, solution (2.3) was not used for estimating $\mathrm{Fr}(12)$. At $z = 12$ the Froude number was calculated as $\mathrm{Fr}(12) = \mathrm{Fr}(0)\langle U_z(12)\rangle / D(12)$, where $\langle U_z(12)\rangle$ and $D(12)$ are the mean axial velocity and the jet diameter determined by Eq. (2.1).

In Fig. 2 the mean fields of the vertical and horizontal velocity components and the r.m.s. density fluctuations obtained in the numerical simulation with $\mathrm{Fr}(12) = 1.5$ show that under the action of stratification the jet is decelerated in the vicinity of the pycnocline and penetrates into the upper fluid layer up to a certain height Z_* corresponding to the turn point. From the turn point the fluid in the jet flows downward, thus forming a counter stream with respect to the ascending current, and then spreads in a horizontal plane on the pycnocline level z_0. Thus, in the $z_0 < z < Z_m$ region a fountain is formed.

The results of the calculations show that at $\mathrm{Fr}(0) < 3$ the mean flow in the fountain is steady. With increase in Fr the steady regime loses the stability and the fountain begins to execute low-frequency self-oscillations, which, in turn, generate internal waves in the pycnocline. In Fig. 2c the self-oscillations manifest themselves as considerable density fluctuations in the fountain top region. The fountain wanders in the vicinity of the center of the jet and periodically breaks down generating in the pycnocline internal wave packages which travel from the center toward the computation domain boundaries (Fig. 3).

In numerical simulation the spatially-average frequency spectra Z_i of the isopycnic surface oscillations $Z_{\rho=1.5}(x,\ y) - z_0$ with the density value corresponding to the center of the undisturbed pycnocline $\rho_{\mathrm{ref}}(z_0) = 1.5$ and the internal wave spectra were calculated (Fig. 4). The Z_i spectra were averaged over ten points located on the $-5 < x < 5$ interval of the horizontal axis at $y = 0$ with the same spacings. The internal wave spectra were averaged over nine points located on a circle, 20 dimensionless units in radius, with the center on the fountain axis on the pycnocline horizon $z = z_0 = 15$. In Fig. 4b the broken line marks a maximum

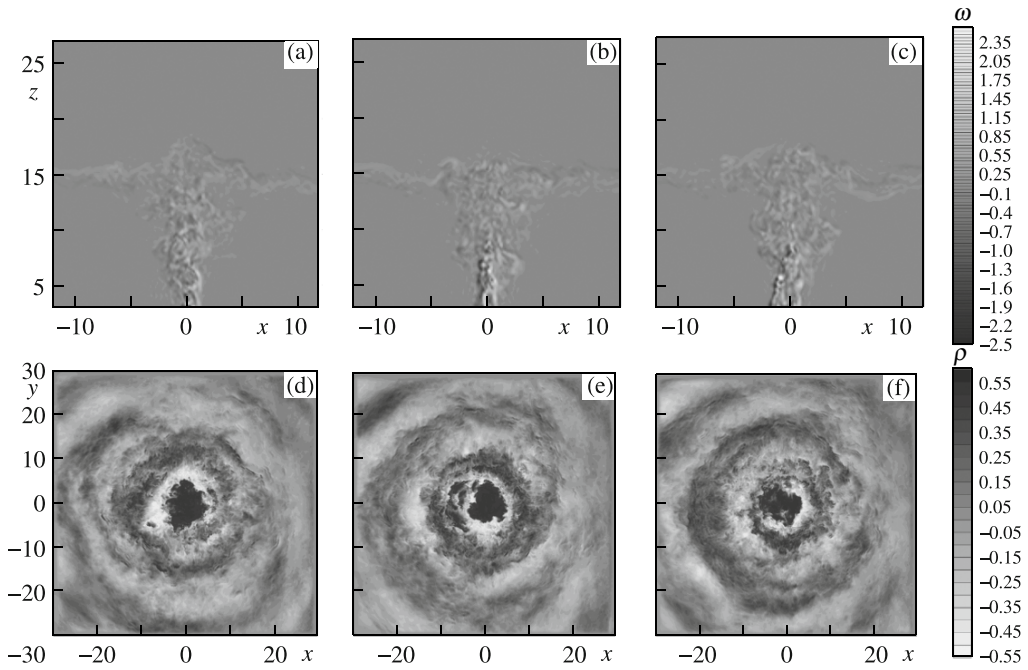

Fig. 3. Distribution of the vorticity component ω_y in the central $(x,\ z)$ plane at the moments $t = 1440$, 1485, and 1530 (a–c) and density deviations from its mean value on the pycnocline horizon in the horizontal $(x,\ y)$ plane at $t = 1530$, 1620, and 1710 (d–f); $\mathrm{Fr}(0) = 11$.

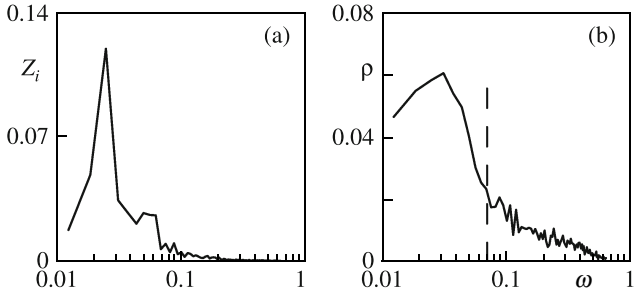

Fig. 4. Spectra of the isopycnic line $\rho = 1.5$ oscillations (a) and the density ρ fluctuations (b) for $\mathrm{Fr}(12) = 1.5$.

of the buoyancy frequency. The results for different Fr show that with increase in the Froude number the frequency of the main peak in the spectra decreases, while the peak amplitude increases. In all the cases the main peak in the internal wave spectra coincides in frequency with the peak in the spectrum Z_i of the density interface oscillations.

To elucidate how the main flow parameters, such as the fountain height, the variance and the characteristic period of the fountain top oscillations, and the internal wave amplitude, depend on Fr the calculations were performed for $3 \le \mathrm{Fr}(0) \le 20$ (Fig. 5).

The fountain height Z_m was determined as a maximum vertical time-average deviation of the isopycnic line $Z_{\rho=1.5}(x,\ y = 0)$ relative to the initial pycnocline level. Clearly that at fairly high Fr ($\mathrm{Fr}(12) > 1$) the fountain height increases with the Froude number as $Z_m \sim \mathrm{Fr}$, which is in agreement with the well-known asymptotics [1] for the turbulent heavy-fluid fountain in a density-homogeneous light fluid.

The variance of the fountain top oscillations Δ_Z was determined from the oscillations of the isopycnic line $Z_{\rho=1.5}(x,\ y = 0)$ and averaged over ten points. In Fig. 5b the behavior of the variance Δ_Z satisfactorily agrees with the steady solution of the Landau equation [19] describing the perturbation amplitude growth in the soft self-excitation regime at a small supercriticity of the form:

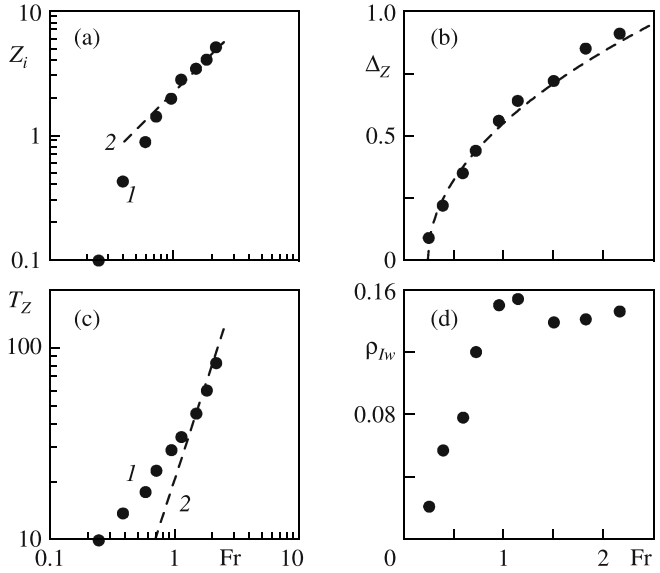

Fig. 5. Fr(12)-dependences of the fountain height Z_m (a), the variance Δ_Z of the isopycnic line $Z_{\rho=1.5}$ displacement in the vicinity of the fountain top (b), the isopycnic line $Z_{\rho=1.5}$ oscillation period T_Z (c), and the internal wave amplitude ρ_{Iw} (d); (*1*) is Z_m and (*2*) is Fr (a) and (*1*) is T_Z and (*2*) is Fr^2 (c).

$$\Delta_Z = (\alpha(\mathrm{Fr} - \mathrm{Fr}_c))^{1/2}, \tag{2.4}$$

where $\alpha = 0.4$ and $\mathrm{Fr}_c = 0.24$ (broken curve in Fig. 5b). Thus, the results of numerical simulation indicate that the steady solution loses the stability owing to the Andronov–Hopf bifurcation leading to the development of an unsteady solution. In this case, the axisymmetric mode of the fountain self-oscillations corresponding to the breakdown regime is predominant (Fig. 3).

The characteristic time scale (period) of the fountain top oscillations was determined from the spectrum Z_i of the isopycnic surface $(Z_{\rho=1.5}(x, y) - z_0)$ oscillations in the form:

$$T_Z = \int Z_i(\omega)\omega^{-1}\, d\omega \Big/ \int Z_i(\omega)\, d\omega. \tag{2.5}$$

As can be seen in Fig. 5c, the fountain top oscillation period monotonically increases with increase in Fr and is proportional to Fr^2 at $\mathrm{Fr}(12) > 1$. These asymptotics are obtained under the assumption that the fountain top oscillation amplitude is determined by the velocity scale U and the buoyancy jump $g\Delta\rho/\rho$. Then for the dimensionless oscillation period we obtain

$$T_Z \sim \frac{\rho U^2}{Dg\Delta\rho} \sim \mathrm{Fr}^2. \tag{2.6}$$

The same asymptotics for the oscillation period of the top of the fountain formed, when a heavy-fluid jet propagates in a homogeneous light fluid, was observable in the experiment [6].

The internal wave amplitudes were determined from the average spectra in the form:

$$\rho_{Iw} = \int \rho(\omega)\, d\omega. \tag{2.7}$$

As can be seen in Fig. 5d, the ρ_{Iw} amplitude increases on the $0.25 < \mathrm{Fr} < 1$ range and varies only slightly at high Fr. The increase in ρ_{Iw} is due to an increase in the fountain top oscillation amplitude, while its saturation is apparently connected with the nonlinear effects including wave breakup.

The results discussed above qualitatively agree with the data of the laboratory experiment [9]. In that experiment the upward-directed $\mathrm{Re} \sim 10^4$ jet flow in a fluid with the temperature stratification in the form of pycnocline was considered. In the pycnocline region the underwater filming of the flow was made, together with the synchronous measurement of the internal waves excited. The experimental results showed that the jet interacting with the pycnocline executed quasiperiodic oscillations in the vertical plane which effectively generated internal waves at frequencies in the vicinity of $0.7N_{\max}$, where $N_{\max}$ is the maximum value of the buoyancy frequency. It was established that the predominant mode is axisymmetric. The numerical results presented in Figs. 3 and 4 are generally in agreement with these experimental data. A more detailed comparison with the experiment is difficult in view of the fact that in the laboratory experiment the pycnocline thickness was of the order of the jet diameter on the pycnocline horizon. In the numerical experiment the dimensionless pycnocline thickness was of the order of unity, that is, much smaller than the jet diameter near the pycnocline horizon $D(12) \approx 5$ (Fig. 2). Moreover, in the laboratory experiment the Reynolds number was almost an order smaller than the value 8×10^4 considered in the numerical simulation, which is very important for the quantitative comparison of the jet oscillation spectra.

Summary. Numerical simulation of the dynamics of a fountain formed, as a turbulent vertical jet penetrates through a pycnocline in a stratified fluid, shows that at the Froude numbers Fr higher than a certain critical value the flow becomes unstable and the fountain executes self-oscillations accompanied by internal wave generation in the pycnocline. The axisymmetric mode is predominant. The internal wave frequency coincides with the fountain top oscillation frequency and decreases with increase in the Froude number. The Fr-dependence of the fountain top oscillation amplitude agrees well with the prediction of the Landau model for the instability mode in the weak self-excitation regime.

The study was carried out with the support of the Russian Foundation for Basic Research (projects Nos. 11-05-00455 and 13-05-91175).

REFERENCES

1. J.S. Turner, "Jets and Plumes with Negative or Reversing Buoyancy," J. Fluid Mech. **26**, 779 (1966).
2. R.C.Y. Koh and N.H. Brooks, "Fluid Mechanics of Waste-Water Disposal in the Ocean," Annu. Rev. Fluid Mech. **7**, 187 (1975).
3. R. Keeler, V. Bondur, and C. Gibson, "Optical Satellite Imagery Detection of Internal Wave Effects from a Submerged Turbulent Outfall in the Stratified Ocean," Geophys. Res. Letters **32**, L12610 (2005).
4. V.G. Bondur, V.M. Zhurbas, and Yu.V. Grebenyuk, "Mathematical Modeling of Turbulent Jets of Depth Waste Water in Coastal Aquatoria," Okeanologiya **46**, 805 (2006).
5. N.B. Kaye and G.R. Hunt, "Weak Fountains," J. Fluid Mech. **558**, 319 (2006).
6. N. Williamson, M. Srinarayana, S.W. Armfield, C.D. McBain, and W. Lin, "Low Reynolds-Number Fountain Behaviour," J. Fluid Mech. **608**, 297 (2008).
7. W. Lin and S.W. Armfield, "Direct Simulation of Weak Axisymmetric Fountains in a Homogeneous Fluid," J. Fluid Mech. **403**, 67 (2000).
8. Yu.I. Troitskaya, D.A. Sergeev, E.V. Ezhova, I.A. Soustova, and V.I. Kazakov, "Internal Wave Self-Generation by Buoyant Jets in a Stratified Reservoir," Dokl. Ross. Akad. Nauk **419**, 691 (2008).
9. E.V. Ezhova, D.A. Sergeev, A.A. Kandaurov, and Yu.I. Troitskaya, "Unsteady Dynamics of Turbulent Axisymmetric Jets in a Stratified Fluid. 1. Experimental Investigation," Izv. Ross. Akad. Nauk. Fizika Atmosfery Okeana **48**, 461 (2012).
10. V.P. Karlikov and O.V. Trushina, "Self-Oscillations of Plane Submerged Fountains," Dokl. Ross. Akad. Nauk **361**, 340 (1998).
11. V.P. Karlikov, S.L. Tolokonnikov, and O.V. Trushina, "Possible Classification of the Self-Oscillatory Spouting Regimes of Plane Vertical Submerged Jets of a Heavy Fluid," Fluid Dynamics **44** (3), 351 (2009).
12. O.A. Druzhinin and O.V. Troitskaya, "Internal Wave Generation by a Fountain in a Stratified Fluid," Fluid Dynamics **45**(3), 474 (2010).
13. A.V. Glazunov, "Vortex-Resolving Turbulence Modeling Using Mixed Dynamic Localized Closure. I. Formulation of the Problem, Description of the Model, and Diagnostic Numerical Tests," Izv. Ross. Akad. Nauk. Fizika Atmosfery Okeana **45**, 7 (2009).

14. A. Yoshizawa and K. Horiuti, "A Statistically-Derived Subgrid-Scale KInetic Energy Model for the Large-Eddy Simulation of Turbulent Flows," J. Phys. Soc. Jap. **54**, 2834 (1985).
15. C. Furbey, G. Tabor, H.G. Weller, and A.D. Gosman, "A Comparative Study of Subgrid Scale Models in Homogeneous Isotropic Turbulence," Phys. Fluids **9**, 1416 (1997).
16. O.M. Belotserkovskii, *Numerical Modeling in Continuum Mechanics* [in Russian], Nauka, Moscow (1984).
17. K.A. Brucker and S. Sarkar, "A Comparative Study of Self-Propelled and Towed Wakes in a Stratified Fluid," J. Fluid Mech. **652**, 373 (2010).
18. G.N. Abramovich, T.A. Girshovich, S.Yu. Krasheninnikov, A.N. Sekundov, and I.P. Smirnova, *Theory of Turbulent Jets* [in Russian], Nauka, Moscow (1984).
19. L.D. Landau and E.M. Lifshitz, *Fluid Mechanics*, Pergamon Press, London (1987).